

# We are IntechOpen, the world's leading publisher of Open Access books Built by scientists, for scientists

**4,800**

Open access books available

**122,000**

International authors and editors

**135M**

Downloads

Our authors are among the

**154**

Countries delivered to

**TOP 1%**

most cited scientists

**12.2%**

Contributors from top 500 universities



**WEB OF SCIENCE™**

Selection of our books indexed in the Book Citation Index  
in Web of Science™ Core Collection (BKCI)

Interested in publishing with us?  
Contact [book.department@intechopen.com](mailto:book.department@intechopen.com)

Numbers displayed above are based on latest data collected.

For more information visit [www.intechopen.com](http://www.intechopen.com)



# Electrical Control of Nonlinear TM Modes in Cylindrical Nematic Waveguide

Carlos G. Avendaño<sup>1</sup>, J. Adrian Reyes<sup>2</sup> and Ismael Molina<sup>3</sup>

<sup>1,3</sup>*Autonomous University of Mexico City, G. A. Madero, Mexico D. F.,*

<sup>2</sup>*Institute of Physics, National Autonomous University of Mexico, Mexico D. F., Mexico*

## 1. Introduction

Liquid crystals (LCs) are intermediate phases between the solid and liquid states of matter whose interesting properties are owing mainly to two remarkable characteristics: i) they can flow as a conventional liquid, ii) they possess positional and orientational order just like those of the solid crystals (de Gennes & Prost, 1993). During the last five decades, LCs have been widely used in optoelectronic devices due to the great ability of changing their properties under the stimuli of external agents as temperature, pressure and electromagnetic fields. It is well known that the propagation of an electromagnetic wave through LCs is a phenomenon that exhibits unique optical properties and highly nonlinear effects (Zel'dovich et al., 1980; Tabiryian et al., 1986).

It is an experimentally well established fact that a polarized and sufficiently intense laser beam may distort the initial orientation of a liquid crystal sample reorienting its molecules against the elastic torques producing a new equilibrium orientational configuration. This orientational transition of the same mesophase is the so called optical Fredericksz transition (de Gennes & Prost, 1993). For pure LCs this phenomenon occurs for linear, circular or elliptically polarized beams and, in the reorientation process, different nonlinear dynamical regimes may be achieved (Durbin et al., 1981). The understanding of the underlying physical mechanisms and the prediction of the ensuing changes in the optical properties of the liquid crystals is an active area of research nowadays (Khoo & Wu, 1993; Santamato et al., 1990).

LCs are anisotropic materials and their linear optical properties are described by a symmetric dielectric tensor, instead of a scalar refractive index. Nonetheless, for liquid crystal films where a uniform orientation is achieved, the dielectric tensor is constant and light propagation through the fluid may be described by the usual laws of crystal optics (Born & Wolf, 1975). But for spatially inhomogeneous liquid crystal layers light propagation is much more difficult to describe, essentially due to the fact that there is no general method to solve Maxwell's equations for an arbitrary spatial dependence of the dielectric tensor. However, for important special cases such as the optical phenomena observed in the cholesteric phase, exact solutions and useful approximations have been worked out if light propagates along the helical axis (Oseen, 1933). For light propagation in an arbitrary direction relative to the helix, the description is more difficult. For this situation Berreman and Scheffer developed a numerical method to solve Maxwell's equations. This method can

be applied to any system where the director changes only in one direction, i. e., for a stratified medium (Berreman & Scheffer, 1970; Shelton & Shen, 1972). But since numerical methods give little insight into the physical features of the problem, approximate solutions of Maxwell's equations have been developed mostly in the context of light propagation in cholesterics. One of these cases is the geometrical optics approximation for LC. This approximation has been formulated in terms of the concept of adiabatic propagation for an arbitrary stratified medium (Allia et al., 1987), or for the case of normal incidence and small birefringence (Santamato & Shen, 1987). On the other hand, a rigorous treatment of the geometrical optics approximation in the special case of a stratified layer with its director oriented everywhere in the plane of incidence of the beam, was presented by Ong (Ong, 1987). But apparently, the generalization of the adiabatic or geometrical optics approximations have not been extended for two or three dimensional spatial variations of the director.

When a high intensity beam is propagated in LCs whose configuration is not anchored to waveguide boundary conditions, give rise to spatial patterns and solitons as a result of the balance between the nonlinear refraction and the spatial diffraction. It is shown that for nematic LCs the electromagnetic field amplitude at the center of Gaussian beam (inner solution), follows a nonlocal nonlinear Schrödinger equation (McLaughlin et al., 1996). For cholesteric LCs and wavelengths outside of the bandgap, it is found that under special conditions the nonlinear coupled equations for the wavepackets in the sample reduces to an extended nonlinear Schrödinger equation with space-dependent coefficients (Avendaño & Reyes, 2004), whereas for wavelengths within the bandgap (stationary waves) the vectorial equation reduces to an extended real Ginzburg-Landau equation (Avendaño & Reyes, 2006). In this system the energy exchanging among the four different modes generated in the sample due to linear and nonlinear coupling is also studied.

It is worth mentioning that the analyses made in the above cited works, the nonlinear effects are obtained in regions of the system where both orientational and optical field have lost influence from the boundary conditions and they have to satisfy only certain mean-field matching conditions. Indeed, as long as the confining cell of the liquid crystal turns to be larger, the bias-free confinement is more notorious.

If the boundary conditions are to be considered, the study of transverse magnetic (TM) nonlinear modes in nematic LC core waveguides can be realized by two different assumptions: i) by assuming hard anchoring boundary conditions for the nematic director, an iterative numerical scheme permits determine up to certain approaches the propagation constant as a function of optical power (Lin & Palffy-Muhoray, 1994), ii) by considering soft anchoring boundary conditions, a numerical but exact procedure allows to obtain the propagating parameters, transverse field distribution and nematic configuration as a function of the mode intensity (Avendaño & Reyes, 2010). It is shown that the anisotropy of the nematic and the intensity of the propagating beam causes simultaneously spatial redistribution of the field amplitude and the nematic configuration, as well as changes in the propagation constant and on the cut off frequencies. As said above, LCs change their properties under external stimuli, so that, it is expected that any external agent will permit us to control these nonlinear parameters.

In next section we review some aspects of the propagation of light in inhomogeneous nematic liquid crystal waveguide consisting of an isotropic core and a quiescent nematic liquid crystal cladding. To this end an analytic and iterative solution of the nematodynamic

equations coupled to Maxwell's equations describing the propagation of a narrow wavepacket, is provided. To cubic order in the coupling between the optical field and the non-stationary reorientational states of the nematic, a perturbed Nonlinear Schrödinger Equation (NLS) is derived. This envelope equation that takes into account the dissipative effects due to the presence of hydrodynamic flow in a cylindrical fiber whose nematic cladding is initially quiescent, and the dissipation associated with the reorientation are also analyzed.

In last section we are focussed in analyzing the effect of applying an axial uniform electric field  $E^{dc}$  on the nonlinear TM modes, the propagating parameters and nematic core configuration by assuming soft anchoring boundary conditions within a cylindrical waveguide made of a nematic liquid crystal core and isotropic cladding. In order to achieve this goal, Maxwell equations are written for the proposed system and their corresponding boundary conditions. Then, we establish the set of nonlinear coupled equations governing the nematic configuration and the transverse field distribution by including the arbitrary anchoring conditions under the action of the uniform electric field applied axially. After this, we solve numerically the coupled nematic-electromagnetic field system and find simultaneously the distorted textures of the nematic inside the cylinder and the nonlinear TM modes as a function of  $E^{dc}$ . We show that the correlation in the spatial distribution of nematic's configuration and nonlinear TM modes, the nonlinear cut-off frequencies and dispersion relations can be tuned by varying the external electric field  $E^{dc}$ .

## 2. Liquid crystal cladding waveguide

We first consider a cylindrical geometry for an optical fiber that takes into account the nonlocal features of the reorientation dynamics. In what follows the coupled time evolution equation for both, the Transverse Magnetic TM modes and for the orientational configuration are derived in an explicit retarded form in terms of the coupling parameter  $q$ , which it will be defined later.

Then, these general equations are solved to linear order in  $q$  for the final stationary orientational configuration and are then used to construct the propagation equation of a wavepacket of TM modes. It is shown that the envelope of the wavepacket obeys a NLS equation which balances self-focussing, dispersion and diffraction in the nematic. For the soliton solution we calculate its speed, time and length scales, and nonlinear index of refraction. They are estimated by using experimental values for some of the parameters (Chen & Chen, 1994).

### 2.1 Coupled dynamics

Let us consider a cylindrical waveguide with an isotropic core of radius  $a$ , dielectric constant  $\epsilon_c$  and a quiescent nematic liquid crystal cladding of radius  $b$  satisfying planar axial boundary hard-anchoring conditions  $\hat{n}(r = a, z) = e_z$ .

The nematic director is written in terms of the angle  $\theta$  as follows

$$\hat{n}(r, z) = \sin \theta \hat{e}_r + \cos \theta \hat{e}_z, \quad (1)$$

where  $\hat{e}_r$  and  $\hat{e}_z$  are the unit cylindrical vectors along the  $r$  and  $z$  directions, respectively. If the reorientation process is isothermal, the equilibrium orientational configurations are determined by minimizing the corresponding total Helmholtz free energy (Frank, 1958)

$$F = (1/2) \int dV \left[ K_1 (\nabla \cdot \hat{n})^2 + K_2 (\hat{n} \cdot \nabla \times \hat{n} + \nu)^2 + K_3 (\hat{n} \times \nabla \times \hat{n})^2 - \mathbf{D}(\mathbf{r}, t) \cdot \mathbf{E}(\mathbf{r}, t) \right] \\ = (1/2) \int dV \left[ K (\nabla \cdot \hat{n})^2 + K (\nabla \times \hat{n})^2 - \mathbf{E}^t(\mathbf{r}, t) \cdot \int dt' \nabla \times \mathbf{H}^*(\mathbf{r}', t') + \mathbf{E}^a(\mathbf{r}, t) \cdot \int dt' \nabla \times \mathbf{H}^*(\mathbf{r}', t') \right], \quad (2)$$

where  $\nu$  is the chirality that we take null for a nematic.  $K_1, K_2$  and  $K_3$  are the splay, twist and bend constants of deformation. Here  $K = K_1 = K_2 = K_3$  is the elastic constant in the equal elastic constant approximation and the asterisk denotes complex conjugation. Here we have used the constitutive relation  $\mathbf{D}(\mathbf{r}, \omega) = \varepsilon(\mathbf{r}, \omega) \cdot \mathbf{E}(\mathbf{r}, \omega)$  with  $\varepsilon(\mathbf{r}, \omega) = \varepsilon_0 (\varepsilon_{\perp}(\omega) I + \varepsilon_a(\omega) \hat{n} \hat{n})$ , where  $\varepsilon_0$  is the permittivity of the vacuum,  $\varepsilon_a = \varepsilon_{\parallel} - \varepsilon_{\perp}$  is the dielectric anisotropy, whereas that  $\varepsilon_{\perp}$  and  $\varepsilon_{\parallel}$  are perpendicular and parallel dielectric constants to the optical axis, respectively, and which leads to the retarded relation between  $\mathbf{E}$  and  $\mathbf{D}$  given by

$$\mathbf{E}(\mathbf{r}, t) = \int dt'' \varepsilon(\mathbf{r}, t-t'') \cdot \mathbf{D}(\mathbf{r}, t'') = \mathbf{E}^t(\mathbf{r}, t) + \mathbf{E}^a(\mathbf{r}, t), \quad (3)$$

where  $\mathbf{E}^t$  and  $\mathbf{E}^a$  are electric fields defined by the following nonlocal and retarded relations

$$\mathbf{E}^t(\mathbf{r}, t) = \frac{1}{\varepsilon_0} \int dt' \int dt'' \frac{\nabla \times \mathbf{H}(\mathbf{r}', t')}{\varepsilon_{\perp}(t''-t')}, \quad \mathbf{E}^a(\mathbf{r}, t) = \frac{1}{\varepsilon_0} \int dt' \int dt'' \frac{\varepsilon_a(t''-t') \hat{n} \hat{n} \cdot \nabla \times \mathbf{H}(\mathbf{r}', t')}{\varepsilon_{\parallel} \varepsilon_{\perp}}. \quad (4)$$

In Eqs. (2), (3) and (4) we have substituted  $\mathbf{D}(\mathbf{r}, t)$  in terms of  $\mathbf{H}(\mathbf{r}, \omega)$  by using Ampere-Maxwell's law without sources. For the specific geometry Eq. (2) takes the form

$$F = (1/2) \int r dr \left[ K \left( \frac{\sin \theta}{r} - r \sin \theta \frac{\partial \theta}{\partial z} + \cos \theta \frac{\partial \theta}{\partial r} \right)^2 + K \left( \sin \theta \frac{\partial \theta}{\partial r} + \cos \theta \frac{\partial \theta}{\partial z} \right)^2 \right. \\ \left. - \left( E_r^{a*} \int dt' \frac{\partial H_{\phi}}{\partial z} - E_z^{a*} \int dt' \frac{1}{r} \frac{\partial (r H_{\phi})}{\partial r} \right) + E_r^{i*} \int dt' \frac{\partial H_{\phi}}{\partial z} - E_z^{i*} \int dt' \frac{1}{r} \frac{\partial (r H_{\phi})}{\partial r} \right], \quad (5)$$

If we now minimize Eq. (5) with respect to  $\theta$ , we find the following Euler-Lagrange equation

$$\frac{\delta F}{\delta \theta} = \frac{\partial^2 \theta}{\partial \zeta^2} + \frac{1}{x} \frac{\partial}{\partial x} \left( x \frac{\partial \theta}{\partial x} \right) - \frac{\sin \theta \cos \theta}{x^2} \\ - q^2 \left[ \frac{\cos 2\theta}{x} \left( E_r^{a*} \int dt' \frac{\partial H_{\phi}}{\partial \zeta} + E_z^{a*} \int dt' \frac{1}{x} \frac{\partial (x H_{\phi})}{\partial x} \right) + \frac{\sin 2\theta}{x} \left( -E_r^{i*} \int dt' \frac{\partial H_{\phi}}{\partial z} + E_z^{i*} \int dt' \frac{1}{x} \frac{\partial (x H_{\phi})}{\partial x} \right) \right] = 0, \quad (6)$$

Where  $\zeta = z/a$ ,  $x = r/a$ ,  $H_{\phi} = H_{\phi} / (c \varepsilon_0 E_0)$  with  $c = 1 / (\mu_0 \varepsilon_0)^{1/2}$  where  $\mu_0$  is the magnetic permeability of free space.  $E_i^a = E_i / E_0$ , with  $i = r, z$ , are dimensionless variables and  $q^2 = \varepsilon_0 E_0^2 a^2 / K$  is a dimensionless variable representing the ratio between electric

energy density and elastic one. Notice that we only use the final stationary state for  $\theta$  defined by (6) due to the large difference between the time scales of reorientation and of time variations of the optical field. In this section we ignore all effects due to absorption.

Since only the TM components are coupled with the reorientation, we assume that the optical field is a TM whose electric and magnetic component are  $E_r, E_z$  and  $H_\phi$ . Thus,  $H_\phi$  is governed in general by the nonlinear, nonlocal and retarded equation obtained by substituting Eqs. (4) into Faraday's law, namely,

$$\frac{a^2}{c^2} \frac{\partial^2 H_\phi}{\partial t^2} = - \int dt' \frac{\left( \frac{\partial^2 H_\phi}{\partial \zeta^2} + \frac{\partial^2 H_\phi}{\partial x^2} \right) (t-t')}{\varepsilon_\perp(r', t')} + \frac{\partial^2}{\partial t \partial \zeta} \int dt' \frac{\varepsilon_a(t')}{\varepsilon_\perp \varepsilon_\parallel} \left[ -\sin^2 \theta \frac{\partial H_\phi}{\partial \zeta} + \frac{\sin \theta \cos \theta}{x} \frac{\partial x H_\phi}{\partial x} \right] (t-t') \quad (7)$$

$$- \frac{\partial^2}{\partial t \partial \zeta} \int dt' \frac{\varepsilon_a(t')}{\varepsilon_\perp \varepsilon_\parallel} \left[ -\sin \theta \cos \theta \frac{\partial H_\phi}{\partial \zeta} + \frac{\cos^2 \theta}{x} \frac{\partial x H_\phi}{\partial x} \right] (t-t')$$

Eq. (6) and (7) define a set of coupled equations for the nematic and optical field (Garcia et al., 2000). Next we solve them iteratively in the weakly nonlinear regime.

## 2.2 Linear and weakly nonlinear dynamics

The solution of Eq. (4) to zeroth order in  $q$  and satisfying the axial boundary conditions defined above, is  $\theta^{(0)} = 0$ . Substitution of this solution into Eq. (7) and taking a monochromatic beam of frequency  $\omega$ , we obtain a linear equation for the zeroth order field  $U \equiv H_\phi^{(0)}$  which is given by

$$\left( \frac{\varepsilon_\perp}{x^2} - \varepsilon_\perp \varepsilon_\parallel \left( \frac{\omega a}{c} \right)^2 \right) U - \varepsilon_\parallel \frac{\partial^2 U}{\partial \zeta^2} - \frac{\varepsilon_\perp}{x} \frac{\partial}{\partial x} \left( x \frac{\partial U}{\partial x} \right) = 0 \quad (8)$$

Solving this equation by the method of separation of variables, its propagating solution is given by

$$U = e^{-i\beta a \zeta} A_1 K_1 \left( x \sqrt{\beta^2 a^2 \frac{\varepsilon_\perp}{\varepsilon_\parallel} - \varepsilon_\parallel \left( \frac{\omega_0 a}{c} \right)^2} \right), \quad (9)$$

where  $A_1$  is an arbitrary constant to be determined by using the boundary conditions. Here  $K_1(x)$  is the modified Bessel function of order 1. On the other hand, the monochromatic expression of  $H_\phi^c(r, z)$  in the isotropic dielectric core (Jackson, 1984) finite at the origin is

$$H_\phi^c = e^{-i\beta a \zeta} B_1 J_1 \left( x \sqrt{\beta^2 a^2 - \varepsilon_c \left( \frac{\omega_0 a}{c} \right)^2} \right), \quad (10)$$

where  $J_1(x)$  is the Bessel function of order 1 and  $B_1$  is also an undetermined constant. To find the constants  $A_1$  and  $B_1$ , it is necessary to impose the following boundary conditions over  $H_\phi$  and its derivative at the boundary (Jackson, 1984),

$$H_\phi^c|_{x=1} = U|_{x=1}, dH_\phi^c / dx|_{x=1} = \varepsilon_\perp^{-1} dU / dx|_{x=1}. \quad (11)$$

Thus, by substituting Eqs. (9) and (10) into Eq. (11) we obtain a transcendental equation for the allowed values of  $\beta$  corresponding to each of the permitted modes in the guide.

To obtain the weakly nonlinear equations for  $\theta$  and  $H_\phi$ , we perform another iteration to find their next nonvanishing order corrections in  $q$ . For this purpose we first insert Eq. (9) into Eq. (6) to obtain

$$x \frac{\partial^2 \theta}{\partial \xi^2} + \frac{\partial}{\partial x} \left( x \frac{\partial \theta}{\partial x} \right) - \frac{\sin \theta \cos \theta}{x} - \frac{q^2 \varepsilon_a A_2^2}{\pi \varepsilon_\parallel \varepsilon_\perp} e^{-2\gamma x} \\ \left[ 2\beta a \cos 2\theta + \frac{\sin 2\theta}{4x^2 \varepsilon_\perp} \left[ 4x^2 \left( \beta^2 a^2 \varepsilon_a - \varepsilon_\perp \varepsilon_\parallel \left( \frac{\omega_0 a}{c} \right)^2 \right) + \varepsilon_\perp \right] / \sqrt{\frac{\varepsilon_\parallel}{\varepsilon_\perp} \left( \beta^2 a^2 - \varepsilon_\perp \left( \frac{\omega_0 a}{c} \right)^2 \right)} \right] = 0, \quad (12)$$

and look for a solution of the form

$$\theta = \theta^{(0)} + q^2 |A(\zeta, t) U(x, t)|^2 \theta^{(1)}(r) + \dots \quad (13)$$

where  $A(\zeta, t)$  is a slowly varying function of its arguments. Hence the equation for  $\theta^{(1)}$  takes the form

$$x \frac{\partial^2 \theta^{(1)}}{\partial x^2} + \frac{\partial \theta^{(1)}}{\partial x} - \theta^{(1)} / x - 2(\varepsilon_a \beta a A_2^2 / \pi \varepsilon_\parallel \varepsilon_\perp) e^{-2\gamma x} = 0 \quad (14)$$

and its solution satisfying the hard anchoring homeotropic boundary conditions  $\theta(x=1) = \theta(x=b/a) = 0$  may be written in terms of the exponential integral function; however, the resulting complicated equation can be approximated using the asymptotic expressions of these functions with the result is given by

$$\theta^{(1)}(x, \omega) = \frac{\beta a \varepsilon_a J_1 \left[ \sqrt{\varepsilon_c \left( \frac{\omega_0 a}{c} \right)^2 - (\beta a)^2} \right]}{\pi \varepsilon_\parallel \varepsilon_\perp x (a^2 - b^2)} \left[ (a^2 - b^2) e^{\gamma a(1-x)} + (b^2 - (xa)^2) + e^{\gamma(a-b)} a^2 (1-x^2) \right]. \quad (15)$$

If we now insert this expression into Eq. (8) and expand the result up to first order in  $q$ , we arrive at an equation of the form

$$\hat{L}(\beta, \omega, x) H_\phi + q^2 \hat{N}(H_\phi) = 0 \quad (16)$$

where the linear and nonlinear operators  $\hat{L}$  and  $\hat{N}$  are defined, respectively, by

$$\hat{L}(\beta, \omega, x) = \frac{1}{x^2 \varepsilon_\parallel \varepsilon_\perp} \left[ -\varepsilon_\perp + x^2 \varepsilon_\perp \left[ \varepsilon_\perp \left( \frac{\omega_0 a}{c} \right)^2 - (\beta a)^2 \right] + x \varepsilon_\perp \frac{\partial}{\partial x} + x^2 \varepsilon_\perp \frac{\partial^2}{\partial x^2} \right] \quad (17)$$

and

$$\hat{N} = \frac{\varepsilon_a |A(\zeta)U(x, \omega)|^2}{x\varepsilon_{\parallel}\varepsilon_{\perp}} i\beta a \left[ U\theta^{(1)}(x) + 3x\theta^{(1)}(x) \frac{dU}{dx} + Ux \frac{d\theta^{(1)}(x)}{dx} \right] A. \quad (18)$$

### 2.3 Wavepacket

The explicit Fourier representation of a monochromatic field as the one considered in last section, depends of the frequency as  $\delta(\omega - \omega_0)$ , where  $\delta$  is the delta function. This suggests that a narrow wavepacket centered around the frequency  $\omega_0$  may be expressed in the form:

$$H_{\phi}(x, \zeta, t) = \ddot{A}(\omega - \omega_0, \zeta) e^{i\beta(\omega_0)a\zeta} U_{\phi}(x, \omega_0) + cc., \quad (19)$$

where the function  $A(\omega - \omega_0, \zeta)$  characterizes the distribution of frequencies around  $\omega_0$ . We assume that this distribution has a small dispersion  $q = (\omega - \omega_0) / \omega_0$ . Thus, if the amplitude  $H_{\phi}(x, \zeta, \omega)$  is expanded in a Taylor series around  $\omega = \omega_0$  and the inverse Fourier transform of  $H_{\phi}(x, \zeta, \omega)$  is taken, we arrive at

$$H_{\phi}(x, \zeta, t) = \frac{1}{2\pi} \sum_{n=0}^{\infty} \frac{1}{n!} \frac{d^n}{d\omega^n} U_{\phi}(x, \omega_0) \int (\omega - \omega_0)^n \ddot{A}(\omega - \omega_0, \zeta) e^{-i(\omega - \omega_0)t} d(\omega - \omega_0) e^{i\beta(\omega_0)a\zeta - i\omega_0 t} + cc. \quad (20)$$

Eq. (20) can be written in the more compact form

$$H_{\phi}(x, \zeta, t) = e^{i\beta(\omega_0)a\zeta - i\omega_0 t} U_{\phi}(x, \omega_0 + iq \frac{\partial}{\partial T}) A(\Xi, T) + cc., \quad (21)$$

where  $A(\Xi, T)$  is the Fourier transform of  $A(\omega - \omega_0, \zeta)$  and is a slowly varying function of the variables  $\Xi \equiv q\zeta$  and  $T \equiv qt$ . Due to the coupling between the reorientation and the optical field, it is to be expected that when a monochromatic TM mode propagates along the cell, higher harmonics may be generated. Therefore, we assume that the solution of Eq. (16) can be written as the superposition

$$H_{\phi}(x, \zeta, t) = e^{i\beta(\omega_0)a\zeta - i\omega_0 t} U_{\phi}(x, \omega_0 + iq \frac{\partial}{\partial T}) A(\Xi, T) + q^2 U^{(1)} + q^3 U^{(2)} + cc. \quad (22)$$

The superindices identify the first, second, ..., harmonics. Note that the presence of the powers of  $q$  implies that the contribution of the higher order harmonics are smaller than the dominant term which is itself a small amplitude narrow wavepacket.

To describe the dynamics of the envelope  $A(\Xi, T)$  we substitute Eq. (22) into Eq. (16) and identify the Fourier variables  $i\beta_a = i\beta_{0a} + q\partial / \partial \Xi_1 + q^2 \partial / \partial \Xi_2$  and  $-i\omega = -i\omega_0 + iq\partial / \partial T$ , in consistency with a narrow wavepacket, and where  $Z = q\Xi_1 = q\Xi_2$  are the spatial scales associated with upper harmonic contributions. Expanding the resulting expressions and grouping contributions of the same order in  $q$ , we find the following expressions

$$q : \hat{L}(i\beta_{0a}, -i\omega_0, x) U_{\phi}(x, \omega_0) A = 0. \quad (23)$$

$$q^2 : \left( \hat{L}(i\beta_{0a}, -i\omega_0, x) \frac{\partial U_{\phi}(x, \omega_0)}{\partial \omega} \frac{\partial}{\partial T} + U_{\phi}(x, \omega_0) \left[ \hat{L}_2(i\beta_{0a}, -i\omega_0) \frac{\partial}{\partial T} + \hat{L}_1(i\beta_{0a}, -i\omega_0) \frac{\partial}{\partial \Xi_1} \right] \right) A = \hat{L} U^{(1)}, \quad (24)$$



$$\begin{aligned}
q^3 : & \left( -\frac{1}{2} \hat{L}(i\beta_0 a, -i\omega_0, x) \frac{\partial^2 U_\phi(x, \omega_0)}{\partial \omega^2} \frac{\partial^2}{\partial T^2} + i \frac{\partial U_\phi(x, \omega_0)}{\partial \omega} \hat{L}_2(i\beta_0 a, -i\omega_0) \frac{\partial^2}{\partial T^2} \right. \\
& + \hat{L}_1(i\beta_0 a, -i\omega_0) \frac{\partial^2}{\partial \Xi_1 \partial T} + \frac{U_\phi(x, \omega_0)}{2} \left( \hat{L}_{22}(i\beta_0 a, -i\omega_0, x) \frac{\partial^2}{\partial T^2} + \hat{L}_1(i\beta_0 a, -i\omega_0) \frac{\partial}{\partial \Xi_2} \right. \\
& \left. \left. + \hat{L}_{12}(i\beta_0 a, -i\omega_0) \frac{\partial^2}{\partial \Xi_1 \partial T} + \frac{\hat{L}_{11}(i\beta_0 a, -i\omega_0)}{2} \frac{\partial^2}{\partial \Xi_1^2} \right) \right) A - \hat{N}(U_\phi(x, \omega_0) A) = \hat{L} U^{(2)},
\end{aligned} \quad (25)$$

where  $L_i(i\beta_0 a, -i\omega_0)$ ,  $i = 1, 2$  denotes the derivative of  $L(i\beta_0 a, -i\omega_0)$  with respect to its first or second argument.

Note Eq. (23) reproduces the usual dispersion relation  $L_i(i\beta_0 a, -i\omega_0) U_\phi(x, \omega_0) = 0$ . Taking the first and second derivatives of Eq. (23) with respect to  $\omega$  we obtain an expression that will allow us to simplify Eqs. (24) and (25) to yield

$$\hat{L}_1(i\beta_0 a, -i\omega_0) U_\phi(x, \omega_0) \left( \frac{ad\beta}{d\omega} \frac{\partial}{\partial T} + \frac{\partial}{\partial \Xi_1} \right) A = \hat{L} U^{(1)}. \quad (26)$$

This expression is a linear inhomogeneous equation  $U_1$ , whose solution is assured to exist by imposing the so called alternative Fredholm condition (Zwillinger, 1989), which is fulfilled if  $LU(r, \omega_0) = 0$  and  $U(r, \omega_0) \rightarrow 0$  as  $r \rightarrow \infty$ . In our case this condition reads

explicitly  $\langle LU^{(1)}, U_\phi \rangle = 0$  and since  $\langle LU^{(1)}, U \rangle \neq 0$ , implies that  $\left( \frac{ad\beta}{d\omega} \frac{\partial}{\partial T} + \frac{\partial}{\partial \Xi_1} \right) A = 0$ ,

which expresses the fact that up to second order in  $q$  the envelope  $A$  travels with the group velocity  $d\beta / d\omega$ .

Similarly by taking the second derivative of Eq. (23), substituting the resulting expression into Eq. (25) together with  $\left( \frac{ad\beta}{d\omega} \frac{\partial}{\partial T} + \frac{\partial}{\partial \Xi_1} \right) A = 0$  it leads to an explicit expression for  $LU^{(2)}$

which upon using again the alternative Fredholm condition  $\langle LU^{(2)}, U_\phi \rangle = 0$ , we find

$$in_2 A |A|^2 + 2 \frac{\partial A}{\partial \Xi_2} + ia \frac{d^2 \beta}{d\omega^2} \frac{\partial^2 A}{\partial T^2} = 0, \quad (27)$$

where the dimensionless refractive index  $\bar{n}_2 = Kn_2 / \varepsilon_0 a^2$  is given by.

$$\begin{aligned}
\bar{n}_2 &= \frac{\varepsilon_a}{\varepsilon_{\parallel}} \left[ \left\langle \frac{U_\phi^3(x, \omega_0)}{x} \frac{dx \theta^{(1)}}{dx}, U_\phi(x, \omega_0) \right\rangle + 3 \left\langle \theta^{(1)} U_\phi^2(x, \omega_0) \frac{dU_\phi(x, \omega_0)}{dx}, U_\phi(x, \omega_0) \right\rangle \right] \\
&= \frac{1}{4} \varepsilon_a^2 \beta a^3 J_1 \left( \frac{a}{c} \sqrt{\varepsilon_c \omega_0^2 - \beta^2 c^2} \right)^3 e^{-\gamma b + 2\gamma a} \frac{ae^{\gamma(a-4b)} - ae^{-3\gamma b} + be^{-\gamma(4a-b)} - be^{-3\gamma a}}{\pi \varepsilon_{\parallel}^2 \varepsilon_{\perp} b (a^2 - b^2) (e^{-2\gamma a} - e^{-2\gamma b})}.
\end{aligned} \quad (28)$$

## 2.4 Soliton dimensions

Using the above expressions, we calculate the values of the properties of the wavepacket, such as the nonlinear contribution  $n_2$  to the refractive index, its coefficient  $d^2\beta/d\omega^2$ , the soliton typical length and time scales and its speed.

For typical values of the dielectric permittivities, from (28) we get a set of values of  $n_2$  (Frank, 1958) corresponding to the allowed values of  $\beta_a$ . The value corresponding to  $\beta_a = 229.59$  is  $n_2^{5CB} = 2.902 \times 10^{-24} (km/V)^2$  which is several orders of magnitude larger than its value for glass,  $n_2^{SiO_2} = 1.2 \times 10^{-28} (Km/V)^2$ . This shows the existence of the giant optical nonlinearity expected for a liquid crystal (Reyes & Rodriguez, 2000). Another physical quantity is the coefficient  $(d^2\beta/d\omega^2)$  of the wavepacket given by the third term of Eq. (27). Using:  $n_o = 1 + n_o^0 + g_o^1 / (\omega_2^2 - \omega^2)$  where  $n_o^0 = 0.4136$ ,  $\omega_1 = 8.9 \times 10^{15} rad/s$ ,  $\omega_2 = 6.68 \times 10^{15} rad/s$ ,  $g_o^0 = 4.8 \times 10^{30} (rad/s)^2$  and  $g_o^2 = 1.66 \times 10^{30} (rad/s)^2$  for 5CB from (Tabiryian et al., 1986), we find that  $(d^2k_{n_o}/d\omega^2)^{5CB} \approx 1.1 \times 10^{-4} ps^2/Km$ . Thus, the width of a picosecond pulse traveling in 5CB in the linear regime is doubled in a distance of 0.1 m; while for glass ( $SiO_2$ ),  $(d^2k_{n_o}/d\omega^2)^{SiO_2} \approx 1.8 ps^2/Km$ , it is doubled in a distance of 0.5 Km. This is consistent with the fact that liquids are considerably more dispersive than solids. Note that Eq. (27) can be rewritten as the NLS equation:  $iA|A|^2 + \partial A/\partial \Xi_2 + i\partial^2 A/\partial T^2 = 0$ , by using the dimensionless variables  $\Xi \equiv \Xi_2/Z_0$  and  $\bar{T} \equiv T/T_0$ , where  $A_0 \equiv c\epsilon_0 E_0$  is the amplitude of the optical pulse. Here  $Z_0 \equiv \epsilon_{\perp} K / (aA_0^2 \epsilon_a^2)$ ,  $T_0 \equiv (d^2\beta/d\omega^2) 2\epsilon_{\perp} K / (\epsilon_a^2 A_0^2 a)$  are the soliton length and time scales. As is well known, the NLS equation admits soliton type solutions given by (Moloney & Newell, 1992)

$$A = 2A_0 \sec\left[\bar{T} - \bar{Z} dk/d\omega Z_0/T_0\right] e^{ik(\omega_0)Z_0\bar{Z} - i\omega_0\bar{T}T_0}. \quad (29)$$

For a 500mW laser at  $\lambda = 0.5 \mu m$ , with a beam waist of  $10 \mu m$ , the field amplitude is  $A_0^2 = 1.9 \times 10^6 V/m$ . Then by using the materials values given above, the spatial and temporal scales for the pulse turn out to be  $Z_0 = 4.2 \times 10^{-5} m$  and  $T_0 = 0.21 \times 10^{-11} s$ .

From Eq. (30) we find that the soliton propagates with the speed  $\bar{v} = v/c$

$$\bar{v} = (Z_0/T) d\omega/dk = (n/cA_0) \sqrt{\lambda_0 / 2\pi n_2 d^2\beta/d\omega^2}, \quad (30)$$

which for the chosen values of the parameters yields  $v^{nem} = 0.1$ , which is one order of magnitude smaller than the speed of light  $c$  in vacuum, and roughly has the same value as for glass,  $v^{SiO_2} = 2.5 \times 10^{-1}$ . The difference between  $v^{nem}$  and  $v^{SiO_2}$  comes from the product  $n_2 d^2(kn_o)/d\omega^2$  in Eq. (27), which measures the balance between nonlinearity and dispersion.

## 3. Electrical control of nonlinear TM modes in cylindrical liquid crystal core waveguide

It is important to stress that spatial solitons (Long et al., 2007) found in nonlinear systems are coherent structures formed in regions of the system where both orientational and optical fields have lost influence from the boundary conditions. In this sense, all these balanced and

robust profiles of energy, called solitons, are asymptotic solutions which are not to be forced by strict boundary conditions but they have to satisfy only certain mean-field matching conditions. In this section we are interested instead in analyze the role played by the boundary conditions within the optical- orientational non linear coupling of a liquid crystal cylindrical waveguide.

Most of the optical calculations in waveguides have been done by assuming hard anchoring boundary conditions for the nematic director. This is inconsistent with the high intensity of the propagating TM mode since in the cylinder wall the electric force can be stronger than the surface elastic force as has been shown before for this geometry (Corella-Madueño et al., 2008). Moreover, when liquid crystals are confined to small cavities, its effect is found to be significant, particularly when elastic energies imposed by the confining volume compete with molecular anchoring energies (Corella-Madueño & Reyes, 2008). Hence we cannot ignore surface elastic terms compared with both bulk elastic terms and electric bulk contributions.

In this section we analyze the behavior of a LC nematic confined within a cylindrical fiber of uniform dielectric cladding in which a high intensity TM mode is propagating and a transversal uniform electric field is axially applied on the system. Our aim is to discern how its propagating parameters, transverse field distribution and nematic configuration depend on the optical mode intensity and the external field amplitude, by assuming soft anchoring boundary conditions.

### 3.1 Transverse magnetic field

We assume homeotropic anchoring of the nematic LCs molecules at the cylinder wall. For infinite circular cylinders the symmetry implies that  $\theta$  only depends on the radial distance  $r$  and the director is given by Eq. (1) (see Fig. 1).

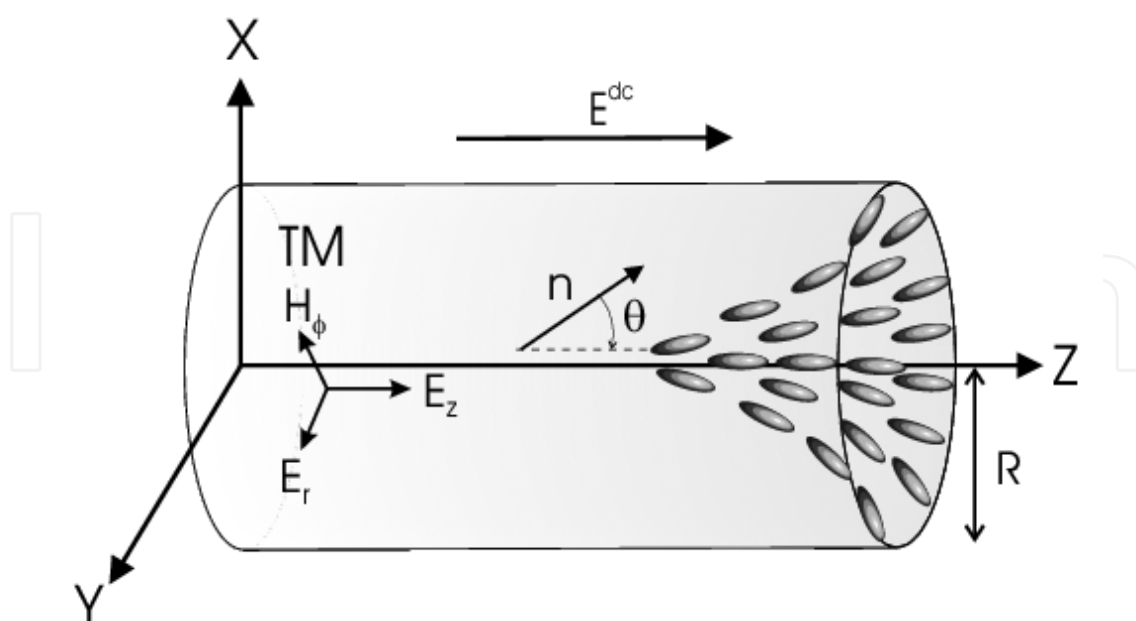


Fig. 1. Cylindrical fiber infiltrated by a nematic liquid crystal and subject to the action of an axial uniform electric field  $E^{dc}$  applied along  $z$  - axis. Also, an optical field of incident electrical amplitude  $E_0$  is propagating through the sample.

As usual,  $TM_{lm}$  and  $TE_{lm}$  propagating modes are considered in studying waveguides, nevertheless, as shown in (Lin & Palffy-Muhoray, 1994), for  $TE_{lm}$  modes the anisotropy and inhomogeneity of the core does not enter into Maxwell's equations. For these modes the resulting equation is equivalent to that of isotropic and homogeneous cylindrical waveguide (Jackson, 1984). We concentrate on  $TM_{lm}$  modes for which the amplitudes of the transverse fields are azimuthally symmetric ( $l = 0$ ). To find the equations governing the propagation of electromagnetic waves through the nematic fiber we assume monochromatic electric  $E_r, E_z$  and magnetic  $H_\phi$  fields propagating along the cylinder of the form:

$$(E_r, E_z, H_\phi) = (e_r, e_z, h_\phi) e^{i(\beta z - i\omega t)} \quad (31)$$

where the dimensionless field components are given by the following expression  $(e_r, e_z, h_\phi) = E_0(G_r(r, k_0), iG_z(r, k_0), F_\phi(r, k_0)/c) e^{-if}$  and  $E_0$  is the incident electric field amplitude. Here we have explicitly separated the phase  $f$  and real valued amplitudes  $G_r(r, k_0)$   $F_\phi(r, k_0)$  of the mode components to simplify the resulting equations. Inserting these expressions into Maxwell's equations and separating real and imaginary parts we find (Corella-Madueño & Reyes, 2006):

$$\frac{dG_z}{dx} = -k_0 R \frac{\epsilon_{rr} - p^2}{\epsilon_{rr}} F_\phi \quad (32)$$

$$G_z = \frac{1}{k_0 R \epsilon_\perp \epsilon_\parallel} \frac{\epsilon_{rr}}{x} \frac{d(xF_\phi)}{dx} \quad (33)$$

$$G_r = \frac{pF_\phi}{\epsilon_{rr}} - \frac{i\epsilon_{rz}}{\epsilon_{rr}} G_z \quad (34)$$

$$\frac{df}{dx} = \frac{pk_0 R \epsilon_{rz}}{\epsilon_{rr}}, \quad (35)$$

where  $x \equiv r/R$ ,  $R$  is the cylinder radius and  $p \equiv \beta/k_0$ , being  $\beta$  the propagation constant. Note that Eqs. (32) and (33) define a self-adjoint equation for  $F_\phi$  so that their eigenvalues  $p$  are real, whereas Eq.(35) provides a phase proportional to the only non diagonal entry of  $\epsilon$ .

To solve exactly the  $TM_{0m}$  modes we shall assume that the nematic cylinder is surrounded by an infinite homogeneous and isotropic cladding of dielectric constant  $\epsilon_c$ . In this way the electromagnetic fields should satisfy the boundary conditions analogous to those given by Eqs. (11):  $h_\phi(x=1, k_0) = h_\phi^c(x=1, k_0)$ ;  $e_z(x=1, k_0) = e_z^c(x=1, k_0)$  and  $h_\phi(x=0, k_0) = 0$ . Where  $h_\phi^c(x, k_0)$  and  $e_z^c(x, k_0)$  are the magnetic and electric fields in the cladding whose expressions are  $h_\phi^c(x, k_0) = AK_1(xk_0R\sqrt{p^2 - \epsilon_c})$  and  $e_z^c(x, k_0) = -Ak_0R\sqrt{p^2 - \epsilon_c}K_0(xk_0R\sqrt{p^2 - \epsilon_c})$ , where  $K_n(x)$  is the modified Bessel function of order  $n$ . Note that, the condition  $h_\phi(x=0, k_0) = 0$  can be derived by realizing that a Frobenius series of the solution of Eq. (32) and (33) has a vanishing independent term. Then, inserting these definitions into boundary conditions, it turns out to be

$$G_z(1) + F_\phi(1) \varepsilon_{\parallel} \varepsilon_{\perp} k_0 R \sqrt{p^2 - \varepsilon_c} \frac{K_0(k_0 R \sqrt{p^2 - \varepsilon_c})}{K_1(k_0 R \sqrt{p^2 - \varepsilon_c})} = 0 \quad \text{and} \quad F_\phi(0) = 0 \quad (36)$$

The boundary value problem defined by Eqs. (32)-(35), and (36) is twofold: first, it involves coefficients which are real valued functions, and second, it is written in terms of self-adjoint differential operators. Thus, its eigenvalues and eigenfunctions are real.

### 3.2 Nematic configuration

The continuous medium description of the director is governed by the total free energy  $F$  containing the elastic and the optical contributions given by Eq. (2) and the external electric energy after integrating this expression over the cylindrical volume. Then, the free energy per unit length:

$$\begin{aligned} F = & \pi K_1 \int_0^1 \left[ \left( \frac{d\theta}{dx} \right)^2 (\cos^2 \theta + \eta \sin^2 \theta) + \frac{\sin^2 \theta}{x^2} + \frac{2(K_1 - K_{24})}{K_1} \right] x dx \\ & - \pi \varepsilon_{\perp} \int_0^1 (|e_z|^2 + |e_r|^2 + |e_\phi|^2) x dx \\ & - \frac{\pi q K_1}{E_0^2} \int_0^1 [ |e_z|^2 \cos^2 \theta + |e_r|^2 \sin^2 \theta + \frac{\sin 2\theta}{2} \text{Re}[e_r e_r^*] ] x dx \\ & - \pi \lambda K_1 \int_0^1 [ \cos^2 \theta + \varepsilon_{\perp} / \varepsilon_{\parallel} ] x dx + \pi \sigma K_1 R^2 \cos^2 \theta \end{aligned} \quad (37)$$

Where the elastic moduli  $K_1$ ,  $K_2$  and  $K_3$  describe the splay, twist and bend deformations, respectively.  $K_{24}$  is called the surface elastic constant because it is the coefficient of a divergence term which can be transformed to a surface integral by using Gauss theorem. This elastic constant has to be included because analysis of the Frank free energy for nematics confined to cylindrical regions indicates that the director pattern is dependent on the surface elastic constant  $K_{24}$  if there is weak normal anchoring and escape along the cylinder axis (Crawford et al., 1992)  $\eta = K_3 / K_1$ ,  $\sigma = RW_\theta / K_1 + K_{24} / K_1 - 1$  and  $W_\theta$  denotes the strength of interaction between the liquid crystal and the confining surface in units of energy per area. Finally,  $q \equiv \varepsilon_a R^2 E_0^2 / K_1$ , as seen in section 2, define the ratio between the optical energy and the elastic one;  $\lambda \equiv \varepsilon_a R^2 E^{dc2} / K_1$  is another important dimensionless parameter representing the ratio of the external electric and elastic energies; for  $\lambda \ll 1$  the influence of the applied field is weak, whereas for  $\lambda \gg 1$  the field essentially overcomes the Van der Waals forces between the molecules. To illustrate the order of magnitude of the electromagnetic fields involved, we shall calculate the optical power corresponding to  $q = 1$ . Let us assume a fiber radius of  $R = 10 \mu m$ . This assures a strong dependence of both texture and electromagnetic fields on the boundary conditions. This leads to an electric amplitude  $E_0 = 1.3 \times 10^5 V/m$  which has an irradiance equal to  $I = c \varepsilon_{\perp} E_0 / 2 = 2.25 \times 10^7 W/m^2$ . If this energy density is distributed across the transverse area of the cylindrical fiber  $\pi R^2$  we shall obtain a laser power  $P = \pi R^2 I = 7 \times 10^{-3} W$ . The

stationary orientational configuration  $\theta(x)$  is determined by minimizing the free energy. This minimization leads to the Euler-Lagrange equation in the bulk

$$0 = \frac{d^2\theta}{dx^2} x^2 (\cos^2 \theta + \eta \sin^2 \theta) + \left(\frac{d\theta}{dx}\right)^2 \frac{x^2}{2} (\eta - 1) \sin 2\theta + x \frac{d\theta}{dx} (\cos^2 \theta + \eta \sin^2 \theta) - \frac{\sin 2\theta}{2} - q \frac{x^2 \sin 2\theta}{2\varepsilon_{rr}^2} (-p^2 F_\phi^2 + \varepsilon_{\parallel} \varepsilon_{\perp} G_z^2) - \lambda \frac{x^2 \sin 2\theta}{2} \quad (38)$$

to the condition  $\theta(x=0)=0$  in the core and to the arbitrary anchoring boundary condition at the surface

$$d\theta / dx|_{x=1} = (\sigma / 2) \sin 2\theta / (\cos^2 \theta + \sin^2 \theta)|_{x=1} \quad (39)$$

where we have inserted the conditions Eqs. (33) and (34) in the Euler-Lagrange equation.

### 3.3 Solutions

We solve this boundary value problem by using the shooting method in which we employ a Runge Kutta algorithm to solve simultaneously Eqs. (32), (33) and (38) by using as initial conditions the right expression of Eq. (36) and arbitrary value for  $G_z(0)$  in order to search the value of  $p$  and  $\alpha = d\theta / dx|_{x=0}$  for which the conditions stated in Eqs. (36) and (39) are satisfied. Numerical solutions of Eq. (38) were calculated for 5CB at  $T_{IN} - T = 10^\circ\text{C}$  with the transition temperature  $T_{IN} = 35^\circ\text{C}$ ,  $\varepsilon_c = n_c^2 = (1.33)^2$ ,  $\varepsilon_{\perp} = 2.2201$ ,  $\varepsilon_a = 0.636$ ,  $\eta = 1.316$ ,  $\sigma = 4$ ,  $K_1 = 1.2 \times 10^{-11} \text{N}$ ,  $W_\theta / K_1 = 40 \mu\text{m}^{-1}$  and  $K_{24} / K_1 = 1$  (Crawford et al., 1992). Previous works (Lin & Palfy-Muhoray, 1994) solved separately the electromagnetic boundary problem and the orientational one by following an iterative scheme. Nevertheless, this procedure does not allow to observe the strong correlation in the spatial distribution of nematic's configuration and the transverse modes and hides the dependence of both fields on the optical field intensity, which is related to the parameter  $q$ . In addition to this, our procedure permits to observe the influence of the external electric field intensity, which is related to  $\lambda$ , on the optical modes.

#### 3.3.1 Electrical control of linear TM modes

Notice that by setting  $q=0$  in Eq. (38), we are considering the regime of the linear TM optical modes, for which, the textures of the LC are not distorted due to the propagating wave. Then, by varying the parameter  $\lambda$  we have the possibility of controlling electrically the linear TM modes and their propagating parameters.

As it is well known, below a certain values of frequencies  $\omega_c$ , which are called *cut-off* frequencies, the different optical modes are able to escape from the core and they cannot propagate through the sample. Cut-off frequencies  $k_0 R$  as function of the parameter  $\lambda$  are plotted in Fig. 2. Notice that, as  $\lambda$  augments, the cut-off frequencies increases as well. This means that we can electrically control the frequencies for which the modes can be propagated. In fact, any particular propagating mode can be suppressed (or stimulated) by increasing (or decreasing) the external field.

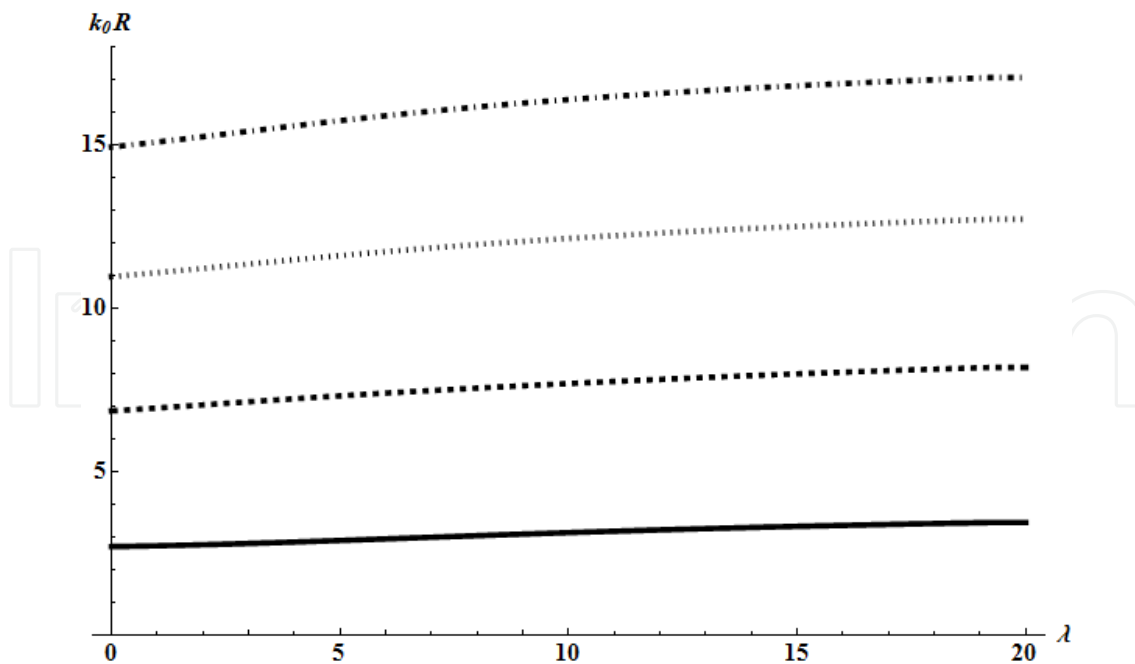


Fig. 2. Cut-off frequencies  $k_0R$  for the zeroth (solid line), first (dashed line), second (dotted line) and third (dot-dashed line) modes versus  $\lambda$ .

In Fig. 3 we plot the slope  $\alpha$  of the angle  $\theta$  at the cylinder axis as function of  $\lambda$ . From this graphic, we see that the values of  $\alpha$  are degenerated, i.e., they adopt the same value of  $\alpha$  for each of the different modes. Additionally, the slope decreases as the external field increases, reaching a limit value,  $\alpha = 0$ , for values greater than  $\lambda \approx 19.3$ .

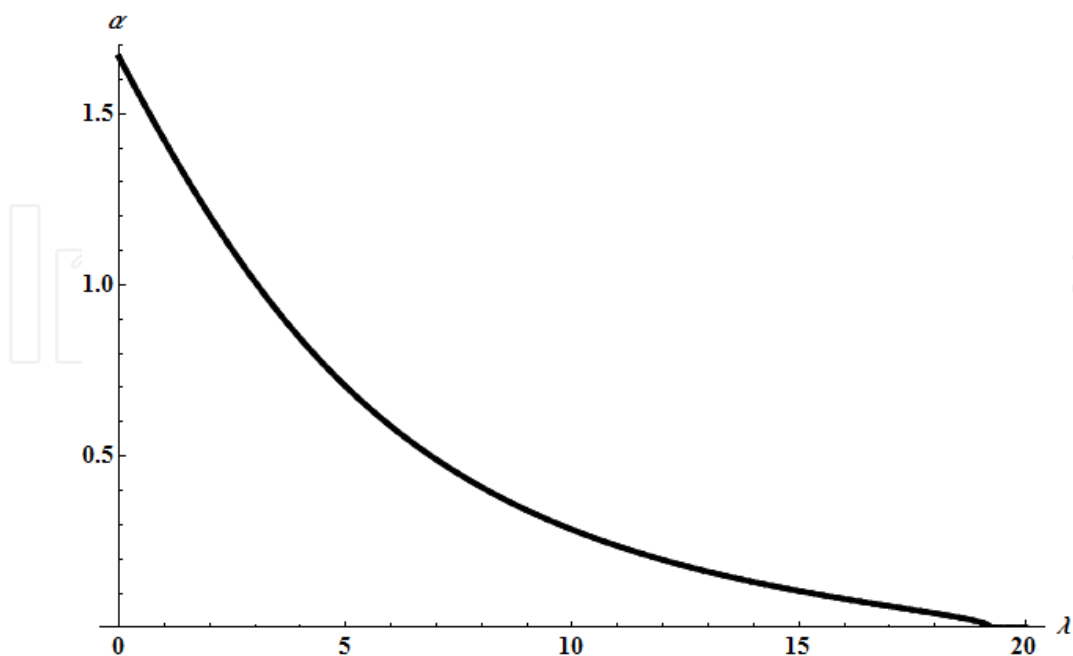


Fig. 3.  $\alpha = d\theta(0) / dx$  against  $\lambda$  for the first fourth modes. These modes coincide for each of the values of  $\lambda$ .

As expected, near the axis, the original escaped configuration,  $\lambda = 0$ , has a higher slope than in the case when the electric field is applied on the waveguide. The effect of the axial electric field  $E^{dc}$  on nematic's molecules is to align them along  $z$ -axis, in such a way, as  $E^{dc}$  gets greater, the slope of  $\theta(x=0)$  becomes smaller each time.

Fig. 4 shows the zeroth mode solutions  $F_\phi$ ,  $G_r$ ,  $G_z$  and  $\theta$  as function of the variable  $x$  at cut-off frequency for different values of  $\lambda$ . Notice how in general, inside the cylinder,  $\theta$  diminishes as  $\lambda$  increases, which implies that the effect of electric field over the initial configuration has major effect for soft anchoring than for strong one. This effect is so notorious that, for sufficiently high values of  $\lambda$ , the nematic configuration  $\theta$  goes to zero for any value of  $x$ . This fact agrees with the Fig. 2, for which, the slope  $\alpha$  is approximately equal to zero, at the nematic axis, for high electric fields. It is clearly shown that as  $\lambda$  gets larger, the amplitudes of  $F_\phi$  and  $G_r$  gets larger as well: in the former case, the maximum amplitude of transverse magnetic field moves to the waveguide axis. This is equivalent to have a higher concentration of energy near the waveguide cladding by augmenting  $\lambda$ .

Finally, the Fig. 5 shows the dispersion relation for the first four modes parametrized by  $\lambda$ . The minimum value of vertical axis takes place at the value  $p = n_c = 1.33$  for which the modes cannot propagate, i. e., at  $p = n_c$  the corresponding values  $k_0R$  are the cut-off frequencies. Particularly, for  $\lambda = 0, 2, 4$ , the first mode cut-off frequencies are  $k_0R = 2.7, 2.75, 2.84$ , respectively.

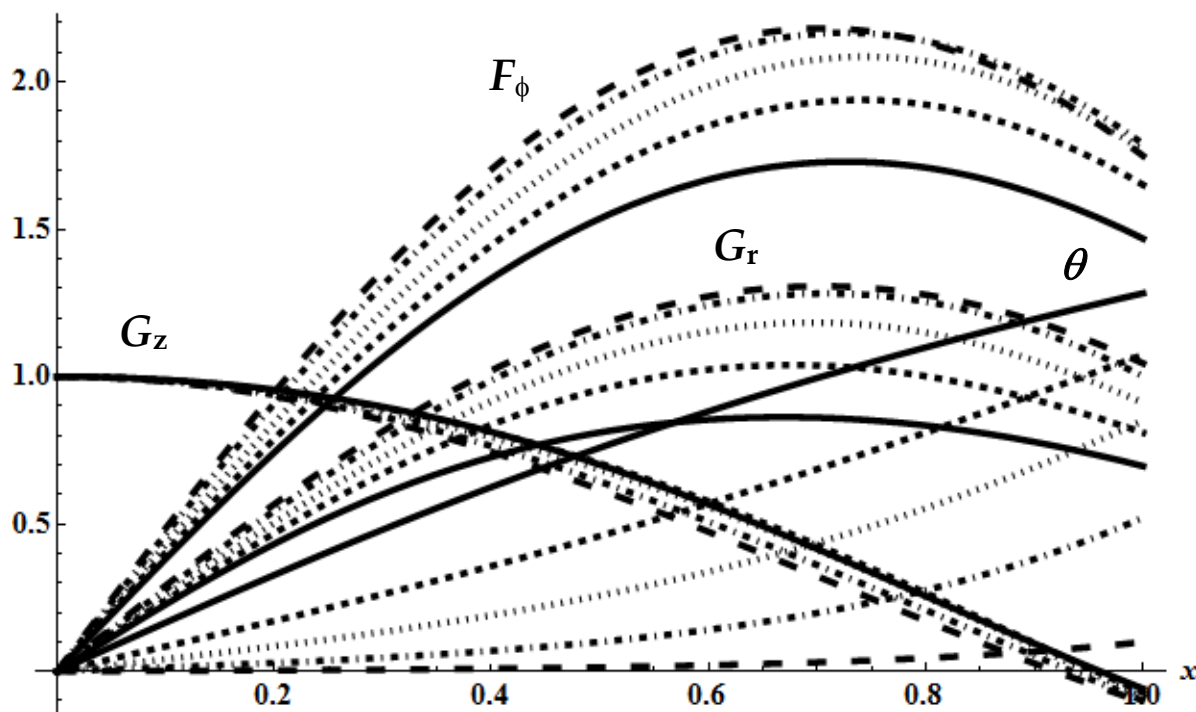


Fig. 4. Dimensionless magnetic and electric fields  $F_\phi$ ,  $G_r$ ,  $G_z$  and director configuration  $\theta$ , at the cut-off frequencies, as function of  $x$  for different values of  $\lambda$ :  $\lambda = 0$  (solid line),  $\lambda = 4$  (dashed line),  $\lambda = 8$  (dotted line),  $\lambda = 14$  (dot-dashed line) and  $\lambda = 19$  (large dashed line).



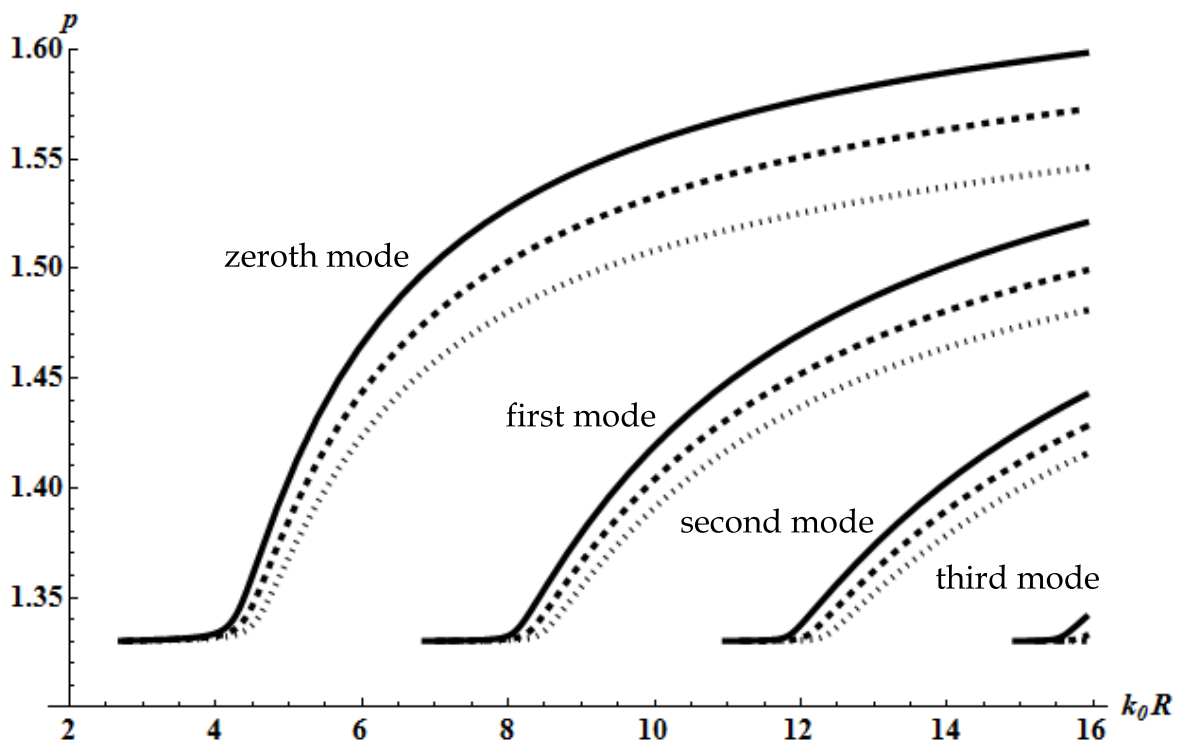


Fig. 5. Dispersion relation  $p$  vs  $k_0R$  for the first four modes at intensities  $\lambda = 0$  (solid line),  $\lambda = 2$  (dashed line) and  $\lambda = 4$  (dotted line). The minimum value of vertical axis takes places at  $p = n_c = 1.33$ .

These results imply that the parameter  $\lambda$  plays an important role in controlling the propagating modes. In fact, as  $\lambda$  increases  $k_0R$  does as well. Thus, for applications in technology, this external electrical control will permit to design waveguides whose propagating modes can be excited or suppressed by varying the external uniform electric field.

### 3.3.2 Nonlinear TM modes

Nonlinear propagating TM modes can be obtained by arbitrarily increasing the intensity value  $q$ . In effect, for values  $q > 0$ , the nematic configuration given by Eq. (38) depends on the electromagnetic wave amplitude. In this subsection we consider the special case  $\lambda = 0$ , for which, the electric field  $E^{dc}$  is absent.

Fig. 6 shows the cut-off frequencies  $\omega_c$  against  $q$  for the first four modes. As  $q$  increases, the cut-off frequencies diminish; and the influence of  $q$  on the cut-off frequencies is sharper for smaller  $q$ -values. Usually, for frequencies  $\omega < \omega_c$ , the corresponding TM mode is not propagating. Thus, by enlarging the intensity of the TM mode  $q$ , this can be conducted by the guide for lower frequencies than for smaller values of  $q$ . However, its influence is reduced when  $q$  is larger than certain value and  $\omega_c$  tends asymptotically to the values shown in this plot. We also notice, by observing Fig. 8, that the influence of  $q$  on the configuration of  $\theta$  is sharper for small values of  $q$ , and hence on the cut-off frequencies. It is worth mentioning that, as mentioned in previous section (see Fig. 2), cut-off frequency values gets larger as external electric field  $\lambda$  increases, whereas, cut-off frequencies diminishes as  $q$  augments.

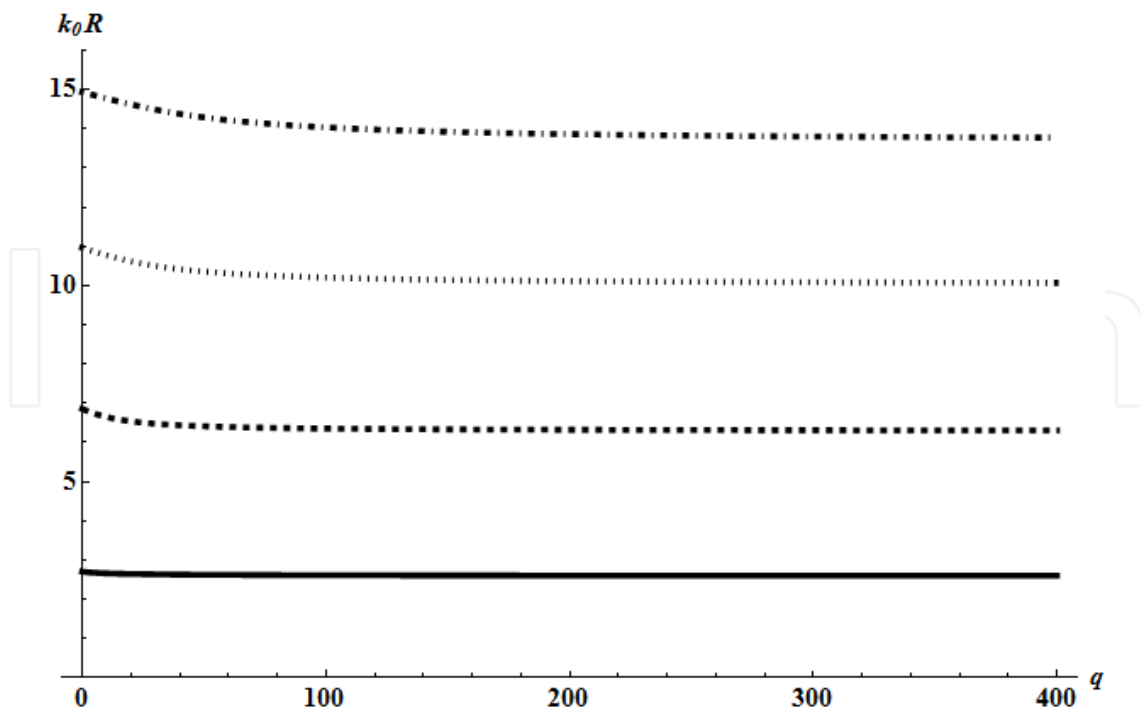


Fig. 6. Cut-off frequencies  $k_0R$  for the zeroth (solid line), first (dashed line), second (dotted line) and third (dot-dashed line) modes versus  $q$ . As it can be seen, the cut-off frequencies  $k_0R$  gets smaller as optical intensity parameter  $q$  gets larger.

Fig. 7 shows the slope  $\alpha$  of the angle  $\theta$  at the cylinder axis as function of  $q$ . Note that, as expected, when the electromagnetic field is absent,  $q=0$ , we obtain only one value for  $\alpha = d\theta(0)/dx$ , corresponding to the equilibrium configuration of nematic known as escaped configuration. For  $q > 0$  the mode amplitude first grows and then decreases against  $q$  for different values of the field for each mode. This happens because for small  $q$ -values the electric field starts to distort the initial escaped configuration, mostly around  $x = 1/2$ .

However, once the electric force overcomes the surface elastic force at the cylinder wall ( $x = 1$ ), the texture is also deformed at the cylinder border and in turn  $\theta$  is also increased.

This causes  $\alpha = d\theta(0)/dx$  to diminish since  $\theta$  is fixed at zero due to the great amount of bulk elastic energy accumulated by the defect of the configuration in the origin.

In Fig. 8 we plot zeroth mode functions  $F_\phi$ ,  $G_r$ ,  $G_z$  and  $\theta$  as function of the variable  $x$  at cut-off frequency for different values of  $q$ . As we can see, the maxima of amplitudes of electric field  $G_r$  and  $G_z$  moves to the cylinder axis, whereas the maximum of amplitude of magnetic field  $F_\phi$  displace to the cylinder border. However, the relative variations of both  $F_\phi$ ,  $G_r$  and  $G_z$  versus  $q$  is negligible in comparison with that of  $\theta$ . This can be understood on the fact that  $F_\phi$ ,  $G_r$  and  $G_z$  fulfill hard boundary conditions whereas  $\theta$  satisfies soft boundary conditions. In other words, by increasing  $q$ , the stationary orientational configuration  $\theta(x)$  at the cylinder border gets larger. Particularly, for  $q = 400$ , the angle  $\theta(x)$  ranges from  $\theta(x=0) = 0^\circ$  to  $\theta(x=1) = 90^\circ$ , that is, like a homeotropic configuration; while, for  $q = 0.001$  the angle  $\theta$  is approximately  $74^\circ$  at the cylinder wall. In other words, as light power increases, the nematic molecules align perpendicular to the cylinder wall. This behavior means that for arbitrary anchoring conditions the field has major effect over

the configuration than for hard-anchoring. In addition to this, we see that away from the axis  $G_r > G_z$ , and the director tends to align in the radial direction as  $q$  grows.

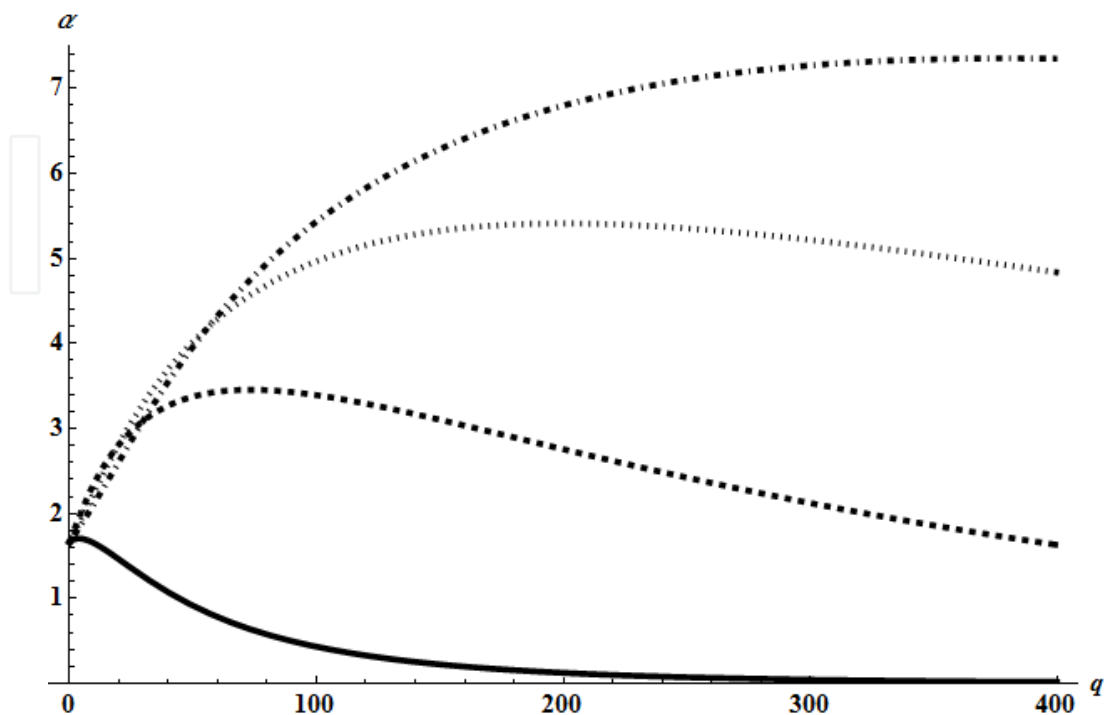


Fig. 7.  $\alpha = d\theta(0)/dx$  against  $q$  for the same modes of Fig. 6. Notice that, when the electromagnetic field is absent,  $q = 0$ , we obtain only one value for  $\alpha = d\theta(0)/dx$ , in agreement with Fig. 3.

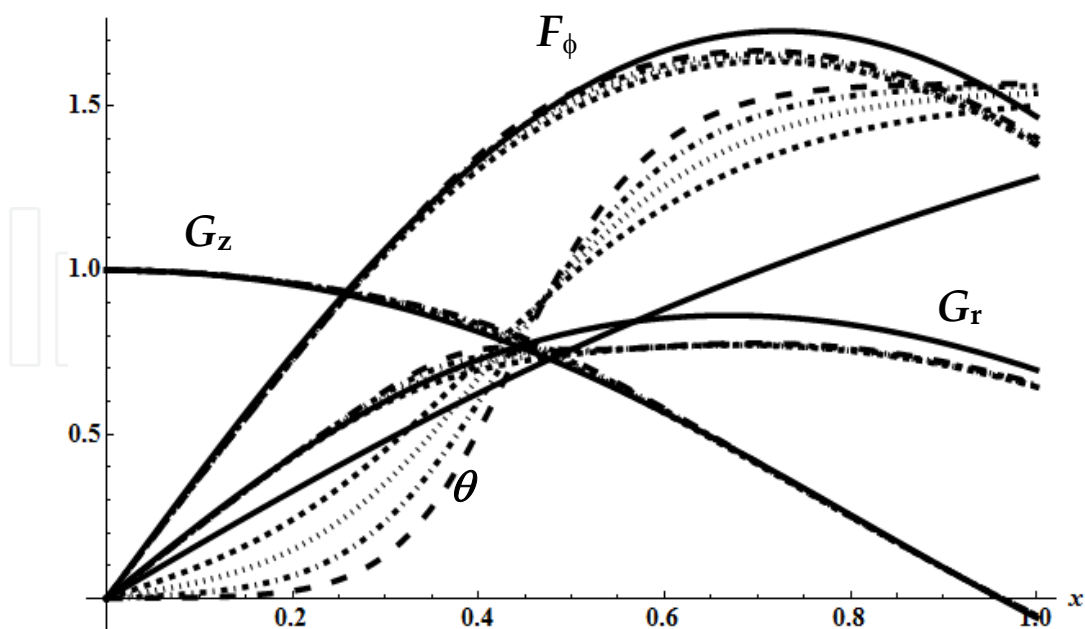


Fig. 8. Dimensionless magnetic and electric fields  $F_\phi$ ,  $G_r$ ,  $G_z$  and director configuration  $\theta$  at the cut-off frequencies, as function of  $x$  for five values of  $q$ :  $q = 0$  (solid line),  $q = 50$  (dashed line),  $q = 100$  (dotted line),  $q = 200$  (dot-dashed line) and  $q = 400$  (large dashed line).

Fig. 9 depicts the dispersion relation for the first four nonlinear modes at three different values of  $q$ . As expected, for all modes, the minimum value of parameter  $p$  is  $n_c = 1.33$ . This occurs just at cut-off frequencies, for which, the ratio  $\beta / k_0$  is simply equal to  $n_c$ . For particular cases  $q$  equal to 0, 5 and 10, the cut-off frequencies  $k_0R$  for the zeroth mode are 2.7, 2.67 and 2.65, respectively. For practical cases, the waveguides are designed so that they can support only the zeroth mode; Fig. 9 can be used for determining some of these useful parameters.

Finally, we mention that, the opposite effect to what we have just said can be seen in Fig. 5, for which the cut-off frequency values gets larger as external electric field  $\lambda$  increases. Therefore, our results show that we can control the propagating or not propagating modes in the waveguide by changing two different parameters: wave amplitude and external electric field.

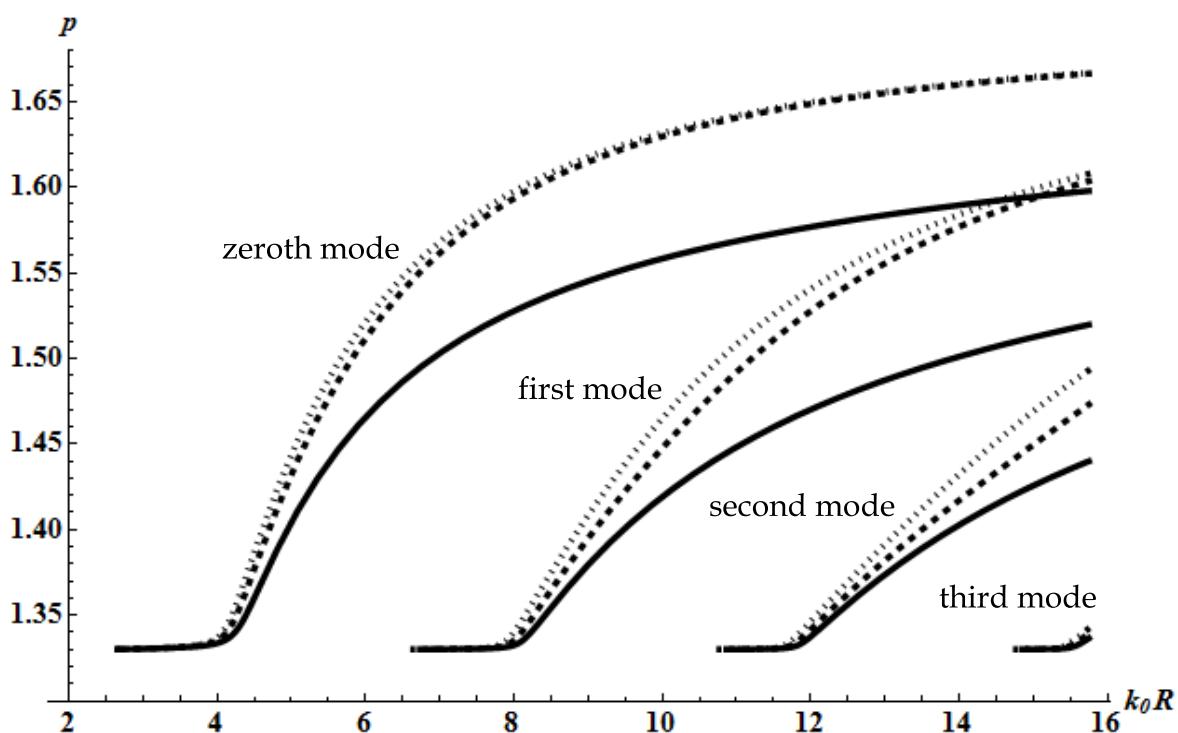


Fig. 9. Dispersion relation  $p$  vs  $k_0R$  for the first four modes at intensities  $q = 0$  (solid line),  $q = 5$  (dashed line) and  $q = 10$  (dotted line). The minimum value of vertical axis takes places at  $p = n_c = 1.33$ .

### 3.3.3 Electrical control of nonlinear TM modes

In the most general case in which  $\lambda \geq 0$  and  $q \geq 0$  we are able to tune nonlinear TM modes by varying the uniform electric field represented by  $E^{dc}$ . It is expected that, nematic configuration, propagating modes, dispersion relation and cut-off frequencies can be adjusted by modifying the applied electrical field and by modulating the amplitude  $E_0$  of propagating optical field. As said above, while the cut-off frequencies depend directly on  $\lambda$ ,  $\omega_c$  depend inversely on parameter  $q$  (see Fig. 2 and Fig. 6). This influence is also observed over the dispersion relation for two different cases: i) the curves acquire larger

values of frequencies  $k_0R$  as external electric field  $\lambda$  increases (see Fig 5), whereas ii) the curves adopt smaller values of frequencies as  $q$  gets higher (Fig. 9). These two controlling parameters have specific roles on the tuning of the different optical properties of the cylindrical waveguide.

In Fig. 10, we plot the same curves of Fig. 5 but now for nonlinear TM modes for which  $q = 10$ .

Notice how the influence of applied field over the relation dispersion is modest in comparison to that of Fig. 5 whose curves were clearly modified by the parameter  $\lambda$ . In this particular case, the strength of transverse modes are striving against axial uniform electric field. This result permit us the tuning of optical nonlinear modes in a more precise manner, since the tuning range of  $\lambda$  for changing cut-off frequencies is wider than for the linear mode.

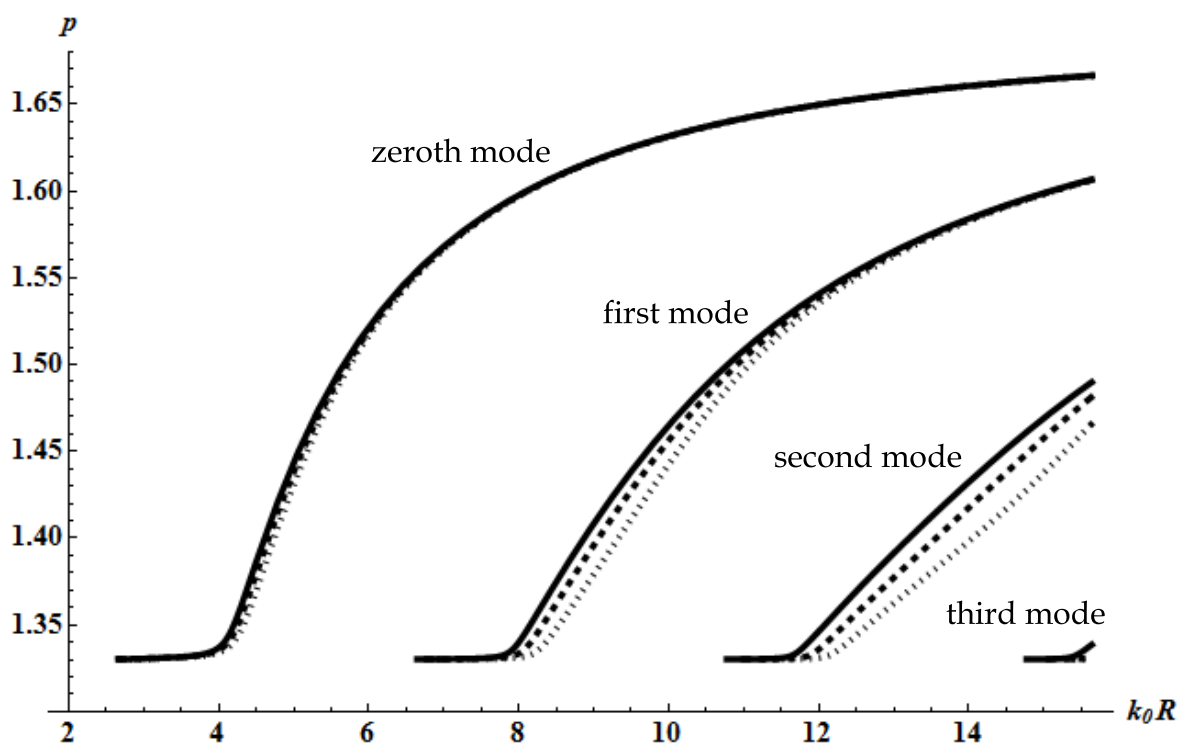


Fig. 10. Dispersion relation  $p$  vs  $k_0R$  for the first four modes at intensities  $\lambda = 0$  (solid line),  $\lambda = 2$  (dashed line) and  $\lambda = 4$  (dotted line). The minimum value of vertical axis takes places at  $p = n_c = 1.33$ .

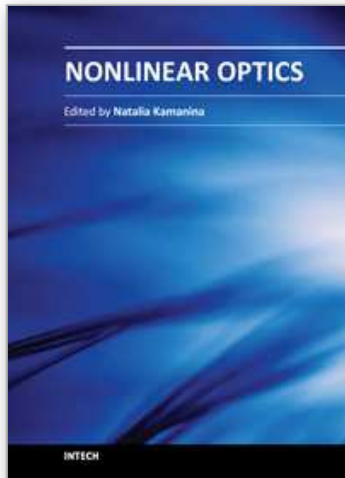
#### 4. References

- Allia P., Oldano C. & Trossi L.(1987). Light propagation in anisotropic stratified media in the quasi adiabatic limit, *Mol. Cryst. Liq. Cryst.* 143, 17-29.
- Avendaño C.G.& Reyes J. A.(2004). Spatial Solitons in Chiral Media *Phys. Rev. E* 70, 061701-1-6.
- Avendaño C.G. & Reyes J. A. (2006). Wave mixing and spatial structures in cholesteric liquid crystals, *Rev. Mex. Fis.*, S 52 ,5, 23-31.
- Avendaño C.G. & Reyes J.A. (2010). Nonlinear TM Modes in a Cylindrical Liquid Crystal Waveguide, *Opt. Commun.* 283, 24, 5016-5020.

- Becchi M., Ponti S., Reyes J. A. & Oldano C. (2004). Defect modes in helical photonic crystals: An analytical approach, *Phys. Rev. B* 70, 033103-7.
- Berreman D.W. & Scheffer T.J. (1970). Reflection and transmission by single-domain cholesteric liquid crystal films: theory and verification, *Mol. Cryst. Liq. Cryst.* 11, 395-405.
- Born M. & Wolf E. (1975). Principles of Optics, Pergamon, Oxford, UK.
- Chen S.-H. & Chen T.-J. (1994). Observation of mode selection in a radially anisotropic cylindrical waveguide with liquid-crystal cladding, *Appl. Phys. Lett.* 64, 1893-1895.
- Corella-Madueño A. & Reyes J. A. (2006). Electrically controlled liquid crystal fiber, *Opt. Commun.* 264, 1, 148-155.
- Corella-Madueño A., Castellanos-Moreno A., Gutiérrez-López S., Rosas R. A., Reyes J. A. (2008). Threshold field for a nematic liquid crystal confined two coaxial cylinders, *Phys. Rev. E* 78, 022701-4.
- Corella-Madueno A. & Reyes J. A. (2008). Hydrodynamically controlled optical propagation in a nematic fiber, *Physica B*, 403, 1949-1955.
- Crawford G. P., Allender D. W. & Doane J. W. (1992). Surface elastic and molecular-anchoring properties of nematic liquid crystals confined to cylindrical cavities, *Phys. Rev. A*, 45, 8693-8708.
- de Gennes P.G & Prost J. (1993). The Physics of Liquid Crystals. Clarendon Press, Oxford, UK.
- Durbin S. D., Arakelian S.M. & Shen Y. R. (1981). Optical-field-induced birefringence and Freedericksz transition in a nematic liquid crystal, *Phys. Rev. Lett.*, 47, 1411-1414.
- Frank F.C. (1958). Liquid crystal. On the theory of liquid crystals, *Faraday Soc. Discuss.* 25, 19-28.
- Garcia C., Garza-Hume C., Minzoni A. A., Reyes J. A., Rodriguez R. F. & Smith N. F. (2000). Active propagation and cut-off for low TM modes in a nonlinear nematic waveguide, *Physica D*, 145, 144-157.
- Jackson D. (1984). Classical Electrodynamics, Wiley, New York.
- Karpierz M.A., Sierakowski M. & Wolinsky T.R. (2002). Light beam propagation in twisted nematics nonlinear waveguides, *Mol. Cryst. Liq. Cryst.*, 375, 313-320.
- Khoo I.C. & S. T. Wu S. T. (1993). Optics and nonlinear optics of liquid crystals, World Scientific, Singapore.
- Lin H. & Palfy-Muhoray P. (1994). Propagation of TM modes in a nonlinear liquid-crystal waveguide, *Opt. Lett.* 19, 436-438.
- Long X.W., Hu W., Zhang T., Guo Q., Lan S. & Gao X.C. (2007). Theoretical investigation of propagation of nonlocal spatial soliton in nematic liquid crystals *Acta Phys. Sin.* 56, 1397-1403
- Marcuvitz N. & Schwinger J. (1951). On the representation of the electric and magnetic fields produced by currents and discontinuities in wave guides I, *J. Appl. Phys.*, 22, 806-819.
- McLaughlin D. W., Muraki D. J. & Shelley M. J. (1996). Self-focussed optical structures in a nematic liquid crystal, *Physica D*, 97, 4, 471-497.
- Moloney A. C. & Newell J. V. (1992). Nonlinear Optics, Addison Wesley, New York.
- Ong H. L. (1987). Wave propagation in layered-inhomogeneous planar anisotropic media: geometrical-optics approximation and its application, *Mol. Cryst. Liq. Cryst.*, 143, 83-87.

- Oseen C. W. (1933). The theory of liquid crystals, *Trans. Faraday Soc.* 29, 883-889.
- Reyes J. A. & Rodriguez R. F. (2000). Pulsed Beams in a Nonlinear Nematic Fiber, *Physica D*, 101, 333-343
- Santamato E., G. Abbate G., Maddalena P. & Marrucci L. (1990). Laser-induced nonlinear dynamics in a nematic liquid-crystal film, *Phys. Rev. Lett.*, 64, 1377-1380.
- Santamato E. and Y. R. Shen Y.R. (1987) Pseudo-Stokes parameter representation of light propagation in layered inhomogeneous uniaxial media in the geometric optics approximation, *J. Opt. Soc. Am.* 4, 356-359.
- Shelton J. W. & Shen Y. R. (1972). Study of Phase-Matched Normal and Umklapp Third-Harmonic- Generation Processes in Cholesteric Liquid Crystals, *Phys. Rev.A*, 5, 1867-1882
- Tabiryan N. V., Sukhov A. V. & Zel'dovich B. Y. (1986). Orientational optical nonlinearity of liquid-crystal, *Mol. Cryst.Liq. Cryst.*, 136, 1-139.
- Zel'dovich B. Y., Pilipetskii N. F., Sukhov A. V. & Tabiryan N. V. (1980). Giant optical nonlinearity in the mesophase of a nematic liquid crystal, *JETP lett.*, 31, 5, 263-267.
- Zwillinger D. (1989). Handbook of Differential Equation, Academic Press, New York

IntechOpen



## **Nonlinear Optics**

Edited by Dr. Natalia Kamanina

ISBN 978-953-51-0131-4

Hard cover, 224 pages

**Publisher** InTech

**Published online** 29, February, 2012

**Published in print edition** February, 2012

Rapid development of optoelectronic devices and laser techniques poses an important task of creating and studying, from one side, the structures capable of effectively converting, modulating, and recording optical data in a wide range of radiation energy densities and frequencies, from another side, the new schemes and approaches capable to activate and simulate the modern features. It is well known that nonlinear optical phenomena and nonlinear optical materials have the promising place to resolve these complicated technical tasks. The advanced idea, approach, and information described in this book will be fruitful for the readers to find a sustainable solution in a fundamental study and in the industry approach. The book can be useful for the students, post-graduate students, engineers, researchers and technical officers of optoelectronic universities and companies.

### **How to reference**

In order to correctly reference this scholarly work, feel free to copy and paste the following:

Carlos G. Avendaño, J. Adrian Reyes and Ismael Molina (2012). Electrical Control of Nonlinear TM Modes in Cylindrical Nematic Waveguide, *Nonlinear Optics*, Dr. Natalia Kamanina (Ed.), ISBN: 978-953-51-0131-4, InTech, Available from: <http://www.intechopen.com/books/nonlinear-optics/electrical-control-of-nonlinear-tm-modes-in-cylindrical-nematic-waveguide>

**INTECH**  
open science | open minds

### **InTech Europe**

University Campus STeP Ri  
Slavka Krautzeka 83/A  
51000 Rijeka, Croatia  
Phone: +385 (51) 770 447  
Fax: +385 (51) 686 166  
[www.intechopen.com](http://www.intechopen.com)

### **InTech China**

Unit 405, Office Block, Hotel Equatorial Shanghai  
No.65, Yan An Road (West), Shanghai, 200040, China  
中国上海市延安西路65号上海国际贵都大饭店办公楼405单元  
Phone: +86-21-62489820  
Fax: +86-21-62489821



© 2012 The Author(s). Licensee IntechOpen. This is an open access article distributed under the terms of the [Creative Commons Attribution 3.0 License](#), which permits unrestricted use, distribution, and reproduction in any medium, provided the original work is properly cited.

IntechOpen

IntechOpen